J. Water Environ. Nanotechnol., 3(3): 191-206 Summer 2018

ORIGINAL RESEARCH PAPER

Synthesis of Mesoporous Fe_3O_4 and Fe_3O_4/C Nanocomposite for Removal of Hazardous Dye from Aqueous Media

Hossein Khoshsang[1], Ali Ghaffarinejad[1,2]*, Hojjat Kazemi[3] , Sedighe Jabarian[1]

[1] Research Laboratory of Real Samples Analysis, Faculty of Chemistry, Iran University of Science and Technology, Tehran, Iran
[2] Electroanalytical Chemistry Research Centre, Iran University of Science and Technology, Tehran, Iran
[3] Research Institute of Petroleum Industry, Tehran, Iran

Received: 2018.03.22 Accepted: 2018.06.05 Published: 2018.07.30

ABSTRACT

The magnetic mesoporous Fe_3O_4 and Fe_3O_4/Carbon Nanocomposite (Fe_3O_4/C) are synthesized by a facile hydrothermal method in one- step and are used for methylene blue dye removal. Nanomaterials are characterized by field-emission scanning electron microscope (FE-SEM), transition electron microscopy (TEM), energy dispersive X-ray spectrometry (EDX), X-ray diffraction (XRD), Fourier transform infrared spectroscopy (FT-IR) and Vibrating sample magnetometry (VSM). The specific surface area of the samples and mean pore diameter were measured via Brunauer–Emmett–Teller (BET) surface area measurement technique. To improve the adsorption performance some important parameters affecting dye removal are optimized. Maximum capacity for methylene blue (MB) adsorption on to Fe_3O_4 and Fe_3O_4/C Nanocomposite is 169.5 and 208.33 mg. g^{-1}, respectively, which compared to some same recent reports, has a better adsorption capacity. Thermodynamic parameters (ΔG^o, ΔH^o and ΔS^o) were calculated and the result showed a spontaneous, endothermic and increase in randomness for dye adsorption. The obtained data has the best fitting with Langmuir isotherm and the kinetic analysis has the best fit by pseudo-second order model.

Keywords: *Adsorption, Environmental, Fe_3O_4/C Nanocomposite, Kinetic Study, Methylene Blue*

How to cite this article
Khoshsang H, Ghaffarinejad A, Kazemi, H, Jabarian, S. Synthesis of Mesoporous Fe_3O_4 and Fe_3O_4/C Nanocamposite for Removal of Hazardous Dye from Aqueous Media. J. Water Environ. Nanotechnol., 2018; 3(3): 191-206.
DOI: 10.22090/jwent.2018.03.001

INTRODUCTION

In recent years, the environmental crisis is a great challenge to human life. One of the examples is dyes that are one important and basic pollutants in water pollution. There are over 100,000 dyes as commercially in the world with more than 7×10^5 tons of dyestuff produced every year worldwide and used extensively in textile dyeing and printing industries. About 15% of the total dyes from various textile and other industries get discharged in wastewater causing extensive pollution [1-4]. The presence of low amounts of dyes in water (less than 1 mg. L^{-1} for some dyes) is highly visible and undesirable for humans, animals, and plants, that at long run lead to dangerous disease like genetic mutations and cancer in living organisms. One of the dyes is methylene blue, which is a heterocyclic aromatic compound and is used in the textile industry such as textile, paper, and leather [5-7].

The harmful of MB dye for humans can be noted as follows; if it can be leading to shortness of breath, produces a burning sensation, vomiting, and gastritis or a great amount of it causes chest pain, headache, sweating too much, painful micturition. And so, it causes heart rate, shock, cyanosis, and jaundice, in humans [8, 9]. Hence, the presence of

* Corresponding Author Email: *Ghaffarinejad@iust.ac.ir*

MB in water is hazardous and its elimination from wastewaters is necessary.

There are various methods for dye removal from wastewaters, including adsorption, membrane filtration, electrochemical treatment, photocatalytic decomposition, advanced oxidation processes, coagulation, flocculation, treatment with ozone and chemical & biological process [10-12]. Among these methods, adsorption is the most effective technique, which some of its advantages are easy to use, low cost and often recoverable for further use[13, 14].

Magnetite (Fe_3O_4) and its composites have been widely synthesized and is a suitable case for removal of dye from waste, the advantage of this material are privileged magnetic properties, chemical stability, nontoxic synthesis, biocompatibility, economic, facile separation from the aqueous solution rather than others sorbents also helping to dye adsorption and increasing efficiently is other role of Fe_3O_4 nanoparticles [15, 16] . There are different methods for the synthesis of magnetic particles (Fe_3O_4) Such as co-precipitation[17, 18], mechanochemical [19], microwave [20], hydrothermal [21], ball mill [22] and combustion, with using a variety of precursors. For example, Cornelia Paˇcurariu and coworkers synthesized Fe_3O_4 nanoparticles (NPs)with combustion method and used for MB removal [23]. Also, magnetic separation of carbon nano-adsorbents has been reported recently and have been proven effective. For example, Datta *et al* used Fe_3O_4/ activated carbon (AC) for adsorption of nicotinic acid from aqueous [24]. Cazetta and coworkers used magnetic activated carbon (MAC) derived from biomass waste for toxic dye removal [25]. In another study, Kakavandi *et al*. synthesized Fe_3O_4/AC magnetic nanoparticles for the removal of aniline from aqueous solution [26]. Du *et al*. applied the carbon/ Fe_3O_4 nanoparticle as an adsorbent for methyl orange removal [27].In another study Kong *et al* synthesized Fe_3O_4/C nanoparticles in two steps with glucose as a carbon source and used for organic dyes removal (MB, Cresol red and Congo red) from aqueous solution [28]. In another work, Luo *et al*. synthesized B-Fe_3O_4/C core-shell composites with a particles size of 500 nm, by using of sodium gluconate as a shell of Fe_3O_4 for dye removal [29] and so phenol removal by MAC prepared through physicochemical activation [30]. Also, some papers report adsorptive removal of malachite green and Rhodamine B dyes [31], Acid Yellow dye [32] and As(III) and As(V) [33] as a heterogeneous catalyst for Fenton oxidation of tetracycline [34] and other applications in supercapacitors [35-37].

Cellulose is a cheap material and so is abundant and available in nature. For this reason, in this study, it was used as a carbon source for the synthesis of the Fe_3O_4/C nanocomposite. In the present work, mesoporous Fe_3O_4/C and Fe_3O_4 nanomaterials were synthesized by facile and one-pot hydrothermal method. The proposed sorbent was used for dye removal from water solutions, which its adsorption capacity compared to same sorbents was considerably improved.

EXPERIMENTAL SECTION

Chemicals

Sodium metaperiodate, microcrystal cellulose (MCC) powder, LiCl, ($FeCl_3.6H_2O$), ($FeCl_2.4H_2O$), KCl, NaCl, Ca $(NO_3)_2$, Mg $(NO_3)_2$ and MB (Scheme 1) were purchased from Merck. All chemicals were analytical grade and were used without any purifications, and all the aqueous solutions were prepared with deionized (DI) water.

Synthesis of Magnetic Nps

In brief, 1.44 g of $FeCl_3{\cdot}6H_2O$ and 0.69 g of $FeCl_2{\cdot}4H_2O$ (with 1:1.5 molar ratio) were simultaneously added in a deoxygenated 60 mL alkaline solution (0.2 M NaOH) with vigorous stirring under an Ar gas flow. Mix up the solution for a few minutes and then sealed by autoclave and placed in an oven at 160 °C for 10 h. The product was a black precipitate, then it is separated by a magnet and washed with DI water and ethanol, and was dried at 60 °C for 12 h in a vacuum oven.

Synthesis of 2, 3-Dialdehyde Cellulose

Oxidation of the cellulose (MCC) by a chemical reaction was conducted with the following instruction, 2 g of cellulose powder, 200 mL of deionized water, 1 g LiCl and 2 g sodium metaperiodate were added to a beaker respectively. The pH of the mixture was adjusted to acidic pH,

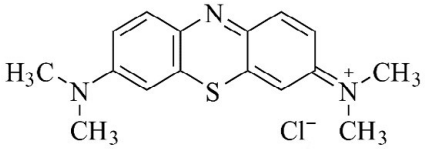

Scheme 1. Chemical structure of MB

and then placed in a dark (to avoid periodate decomposition) and closed vessel at 55 °C was stirred gently for 2-3 h. During this period cellulose is oxidized to 2,3-dialdehyde cellulose (2,3- DAC) (Fig. 1) and this product was filtered with a funnel and then washed with DI water to remove iodine-containing compounds and at the end dried in vacuum oven at 50 °C for 10 h. 2,3-DAC was used for the preparation of Fe_3O_4/C.

Synthesis of Fe_3O_4/C Nanocomposite

0.5 g NaOH was dissolved in 60 mL DI water and 2, 3-DAC obtained from the previous step was stirred and dissolved in this solution to obtain a homogeneous solution. After this, for oxygen removal, Ar inert gas was purged in the solution, and then 0.15 g of $FeCl_2.4H_2O$ and 0.28 g of $FeCl_3.6H_2O$ were added to this solution and mixed for 1 h. Similar to the preparation of Fe_3O_4 NPs the mixture was heated in a Teflon-sealed autoclave in the same conditions preparation of Fe_3O_4.The magnetic materials were collected by a magnet and washed for several times with DI water and ethanol. The final material was dried in an oven with vacuum conditions at 60 °C.

Apparatus

The synthesized materials were characterized by different techniques. Morphology of adsorbent was studied by the FE-SEM model of Hitachi S-4160 operating at 30 kV and TESCAN, Mira III LMU, Czech Republic at 15 KV and TEM images were taken with a model of Zeiss-EM10C (Germany) at 100 KV. FT-IR spectra were obtained by Shimadzu FTIR 8400S spectrometer (Japan). FE-SEM with energy dispersive X-ray spectroscopy (FESEM/EDX, TESCAN, Mira II LMU, Czech Republic) was used for the elemental analysis. XRD patterns were obtained in 2θ between 10 to 80° with a Philips-PW 1800 diffractometer, which was equipped with Cu-Kα irradiation (λ = 0.1524 nm) source. Specific surface area measurements were performed using a standard Brunauer–Emmett–Teller (BET) apparatus (ASAP 2020, micromeritics, USA). Adsorption was carried out at a liquid N_2 temperature at 77 K. Magnetic properties was measured by vibrating sample magnetometry (VSM) analysis (Lakeshore 7410, USA). UV-Vis spectra were obtained with a Shimadzu UV-Visible spectrophotometer model UV-mini 1240 (Japan).

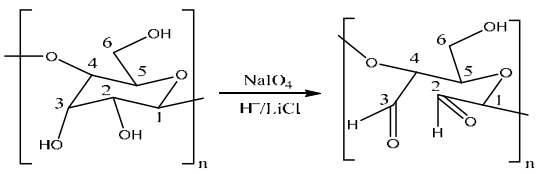

Fig. 1: Oxidation of cellulose (MCC) by sodium metaperiodate

RESULTS AND DISCUSSION

Morphology of Nano Sorbent

The morphology of Fe_3O_4 and Fe_3O_4/C nanomaterials was studied by FE-SEM. Fig. 2 (a-d) illustrates images of these particles with different magnifications. As this Figure shows the Fe_3O_4 and Fe_3O_4/C Nanocomposite are almost cubic and spherical. The TEM images (Fig. 2 (e, f)) obviously show the Fe_3O_4 NPs over carbon structure. With regard to these images, clearly seen that particles size is nanoscale especially in TEM images that size of magnetic nanoparticles is almost 10 nm.

Elemental Analysis

Elemental analysis of the nanomaterials was performed by EDX. Presence of iron, oxygen, and carbon can be observed clearly in the EDX spectrum (Fig. 3). It reveals that the iron is from magnetic Fe_3O_4, the carbon source is from 2,3-DAC and the source of oxygen is related to both samples (Fe_3O_4 and 2, 3-DAC together).

FT-IR Studies

Fig. 4 shows the FT-IR spectra of Fe_3O_4, microcrystal cellulose (MCC) powder, 2, 3 -DAC and Fe_3O_4/C nanocomposite. The bands around 1054 cm^{-1} are related to the C–O stretching vibrations. A small peak near of 2930 cm^{-1} is observed, which illustrates the existence of C–H bonds. In 2,3-DAC the presence of C=O is indicated by the peak at 1737 cm^{-1} and so in 1640 cm^{-1} for Fe_3O_4/C Nanocomposite, and two small peaks about 2850-2950 cm^{-1} are attributed to C-H bonds connected to the carbonyl group. Characteristic bands of Fe–O at 590 cm^{-1} is observed in Fe_3O_4 and Fe_3O_4/C spectra (Fig. 4a, b). A broad peak almost in 3400 cm^{-1} in three samples are assigned to hydroxyl groups [38-40]. A little shift in the position of C=O, C-H and C-O peaks in Fe_3O_4/C sample compared to 2, 3-DAC sample is seen. This shift may be related to the link between C=O, C-H and C-O groups with a Fe_3O_4 structure that decreases the frequency and energy of functional groups bonds and according to the $E=hc\lambda^{-1}$formula the wave number shifts to lower quantities.

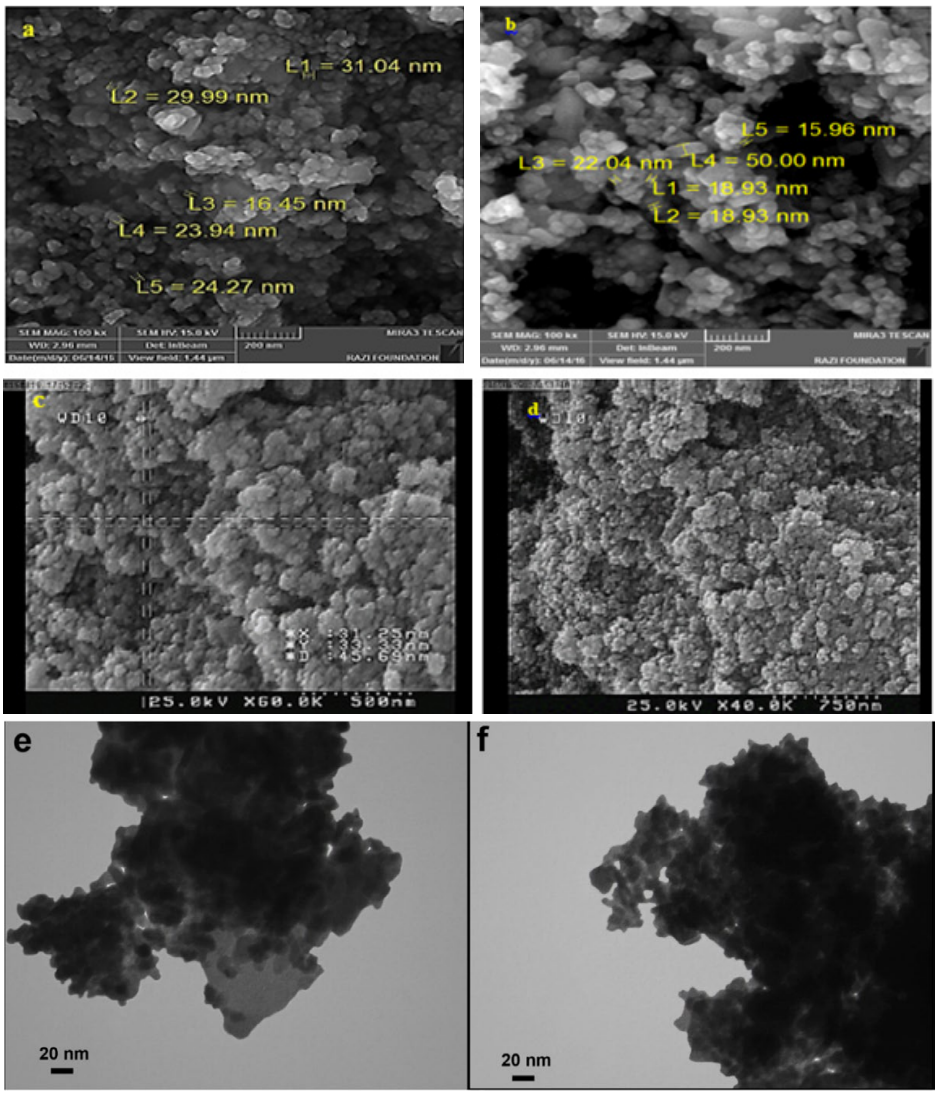

Fig. 2: FE-SEM images of Fe_3O_4 (a, b) and Fe_3O_4/C Nanocomposite (c, d) and TEM images of Fe_3O_4/C Nanocomposite (e, f)

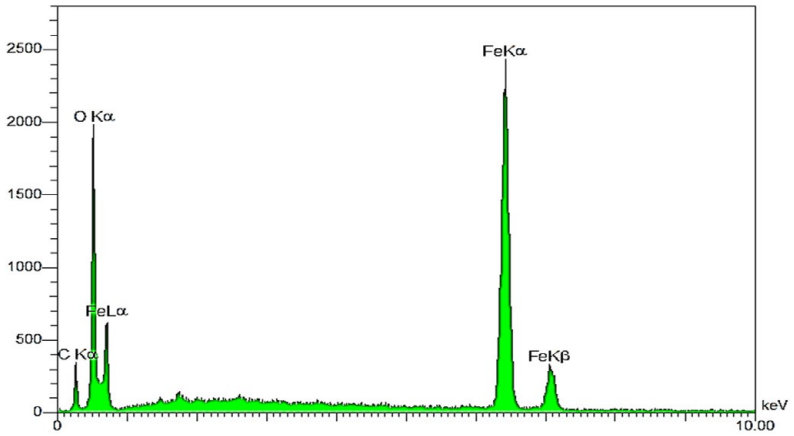

Fig. 3: EDX spectrum of the Fe_3O_4/C nanocomposite.

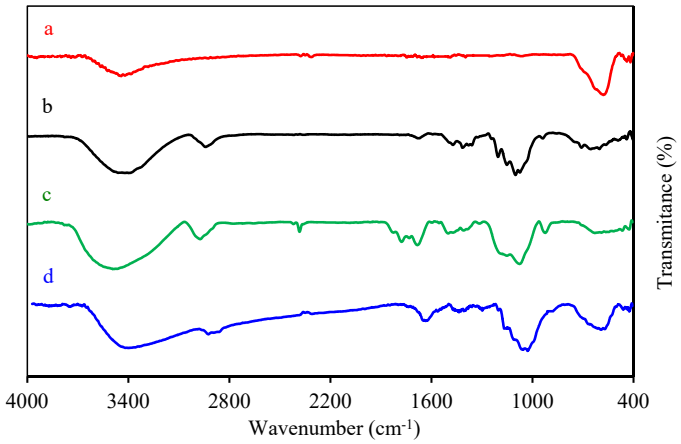

Fig. 4: FT-IR spectra of Fe_3O_4 (a), MCC powder (b), 2, 3-DAC (c) and Fe_3O_4/C Nanocomposite (d)

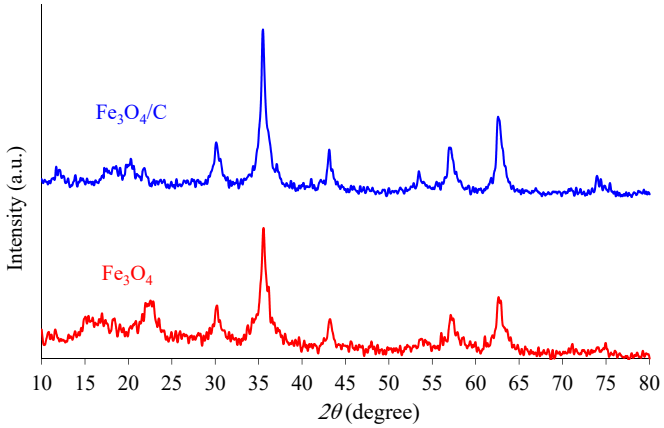

Fig. 5: XRD patterns of Fe_3O_4/C Nanocomposite and Fe_3O_4 NPs

XRD Patterns

Fig. 5 shows the XRD patterns of Fe_3O_4/C Nanocomposite and Fe_3O_4 NPs. The position of all diffraction peaks at 2θ = 75.09, 62.62, 57.02, 53.49, 43.12, 35.48, 30.12 and 18.31° corresponding to (6 2 2), (4 4 0), (5 1 1), (4 2 2), (4 0 0), (3 1 1), (2 0 0) and (1 1 1) of the crystal planes that was indexed to Fe_3O_4 (JCPDS card number 88-0866). The obvious peak between 2θ = 20 to 25° belongs to the carbon structure in Fe_3O_4/C sample.

Because in this study the magnetic crystallites are smaller than 100 nm, the Scherer equation (Eq. 1) can be used for determining and estimating the crystal size.

$$\tau = \frac{k\lambda}{\beta \cos\theta} \quad (1)$$

Where t is the mean size of the ordered (crystalline) domains, which perhaps smaller or equal to the crystal size; k is a shape factor and is a dimensionless quantity and its value is almost 0.9; l is the X-ray wavelength (here λ = 0.154056 nm); b is the line broadening at half the maximum intensity (FWHM), after the instrumental line broadening was subtracted, its unit must be in radians, and q is the Bragg angle in degree. The peak with more intensity (2θ = 35.48°) was selected for crystallite size measurements by Scherer equation, and the average particle size of Fe_3O_4 NPs and Fe_3O_4/C Nanocomposite were 11.9 and 12.9 nm, respectively.

VSM Study

Magnetic NPs was characterized by VSM for determination of magnetic property at room temperature (Fig. 6). The saturation magnetization for Fe_3O_4 NPs is found to be 39.88 emu. g^{-1} and for Fe_3O_4/C is about 14.15 emu. g^{-1}. The obtained

magnetic NPs has a good magnetic potential and could be separated easily from a water solution by a magnet.

N_2 Adsorption/Desorption (BET)

The N_2 adsorption-desorption isotherms curves of Fe_3O_4 NPs and Fe_3O_4/C Nanocomposite was measured at 77 K (Fig. 7a). It is observed that the decrease in the values of surface area for Fe_3O_4 NPs than Fe_3O_4/C Nanocomposite and so loop hysteresis is seen in curves, which indicates samples have mesoporous structure. The measured BET surface areas of the Fe_3O_4 NPs and Fe_3O_4/C Nanocomposite were 7.08 and 26.13 $m^2.g^{-1}$, respectively.

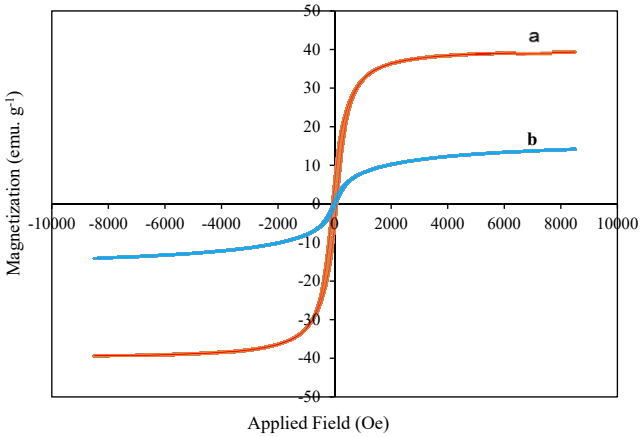

Fig. 6: Magnetization curve of Fe_3O_4 (a) and Fe_3O_4/C Nanocomposite (b)

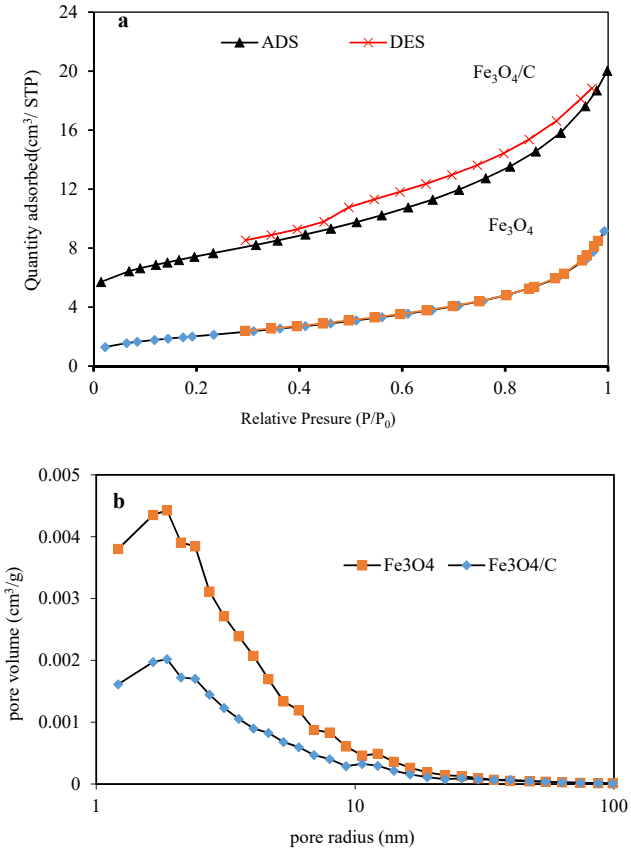

Fig. 7: N_2 adsorption-desorption isotherms (a) and BJH pore-size distribution curves (b)

The pore size distributions obtained from the Barret–Joyner–Halenda (BJH) analysis (Fig. 7b) shows narrow and intensity peaks in the pore size distribution curve that appear in a range of 1 to 10 nm and so indicative a uniform distribution. The total pore volume of the Fe_3O_4 and Fe_3O_4/C are 0.013 and 0.023 $cm^3.g^{-1}$, respectively and the average of the pore size distribution for Fe_3O_4 NPs is 7.85 and for the Fe_3O_4/C Nanocomposite sample is 4.613 nm. The value of the pore diameter indicates that Fe_3O_4/C and Fe_3O_4 are mesoporous materials.

MB Dye Removal Studies

In this work, MB was specified by a UV-spectrophotometer at λ_{max} = 664 nm. The removal percent and adsorption capacity q_e (mg. g^{-1}) were obtained by the following equations:

$$q_e = \frac{(C_0 - C_e)}{m} \quad (2)$$

$$Removal(\%) = \frac{(C_0 - C_e)}{C_0} \times 100 \quad (3)$$

Where, q_e is the adsorption capacity (mg. g^{-1}), C_e (mg. L^{-1}) and C_0 (mg. L^{-1}) is the equilibrium and initial concentrations of MB (mg. L^{-1}), respectively, and m (g) is the adsorbent dosage.

For optimization of dye removal conditions, the effect of some important parameters was studied by one at a time method. In all experiments, during the adsorption process, the mixture of adsorbent and dye solutions were shaken by 200 rpm speed.

Effect of adsorbent dosage

For investigating the effect of the required adsorbent amount, different amounts of Fe_3O_4/C nano-adsorbent in the range of 5 to 20 mg were added to 30 mL of 30 mg. L^{-1} MB solutions. The results of these experiments are illustrated in Fig. 8. As this Figure shows by increasing the amount of adsorbent, the adsorption sites increase and

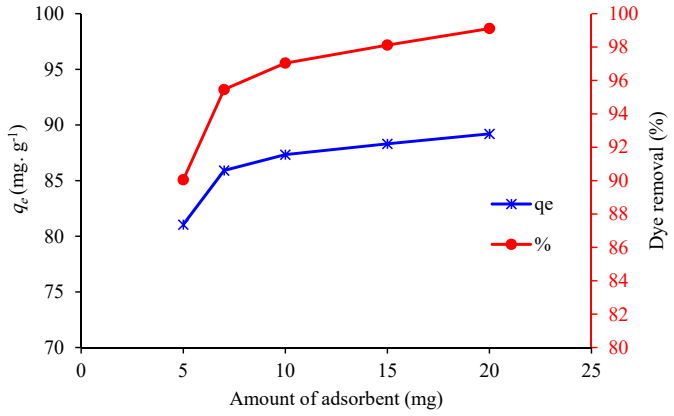

Fig. 8: Effect of adsorbent dosage on MB dye adsorption by Fe_3O_4/C Nanocomposite (C_0 = 30 mg. L^{-1})

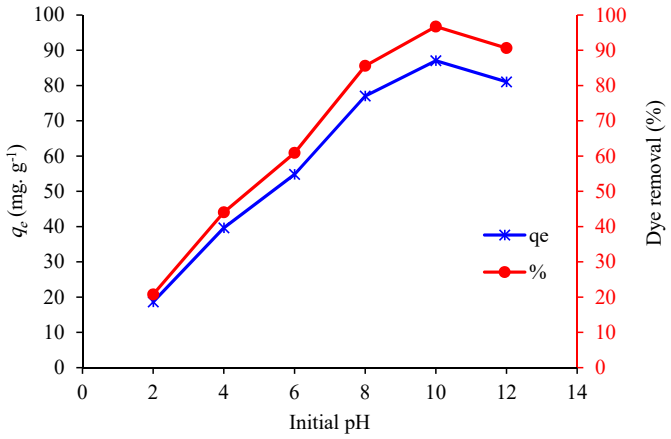

Fig. 9: Effect of initial pH on the adsorption capacities of nanoadsorbent (Fe_3O_4/C) for MB. (C_0 = 30 mg. L^{-1}, solution volume = 30 mL)

consequently the dye removal percent and q_e increase, and in amounts greater than 10 mg of adsorbent these values remain almost constant, which likely the saturation of the adsorbent activated sites. So, for the rest of the experiments, 10 mg of adsorbent was used for dye removal.

Effect of Initial Ph

One of the most influential factors on dye removal is the pH of the solution, which influences on the properties of adsorption and self-adsorption. In this experiment, while C_0 was kept at 30 mg. L^{-1}, the pH was changed (2 - 12 (using 0.1 M NaOH and 0.1 M HCl solutions. Fig. 9. shows the change of q_e and dye removal with pH increasing. As the Figure shows the best result is obtained at pH = 10. In alkaline solutions, the adsorbent has a negative charge and MB has a positive charge. Therefore, their attractive interaction is stronger. Very low adsorption capacity at acidic pHs implied that Fe_3O_4/C nano adsorbent could be renewable at low pH values.

Effect of Ionic Strength

Effect of ionic strength on pollution removal is an important parameter. Because dye wastewater contains various metal ions and salts and presence of this ions cause to increasing of ionic strength. In this study, the influence of four common metal ions (Na^+, K^+, Ca^{2+}, Mg^{2+}) with a concentration of 0.01 M in 30 mL dye solution with pH = 10 was investigated. Fig. 10. shows that salts and metal ions might be adsorbed on Fe_3O_4/C magnetic nano-adsorbent as a competitor, leading to decrease of adsorption capacity, which this decrease is more significant for ions with two positive charges (Ca^{2+} and Mg^{2+}). According to the negative charge of adsorbent, the attraction of more positive charges to it is stronger. The interfering effect of Mg^{2+} can be eliminated by setting pH at higher amounts (pH > 10) because the magnesium ions precipitate at pH > 10.

Influence of Contact Time

The effect of contact time on the MB adsorption was tested to determine equilibrium time for the adsorption process. For this reason, 10 mg of adsorbent was added in 30 mL solution of 30 mg.

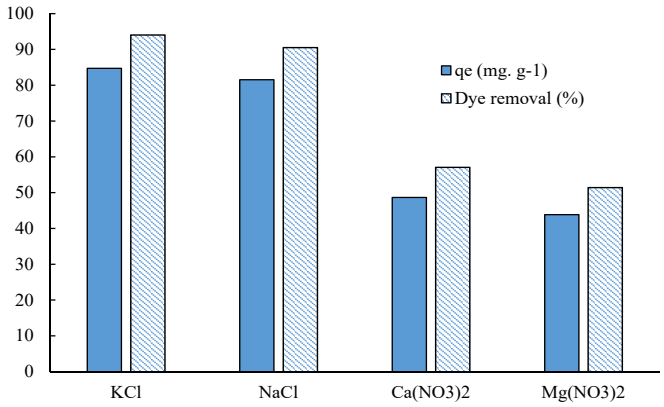

Fig. 10: Effect of various salt on MB adsorption by Fe_3O_4/C Nanocomposite (C_0 = 30 mg. L^{-1}, solution volume = 30 mL)

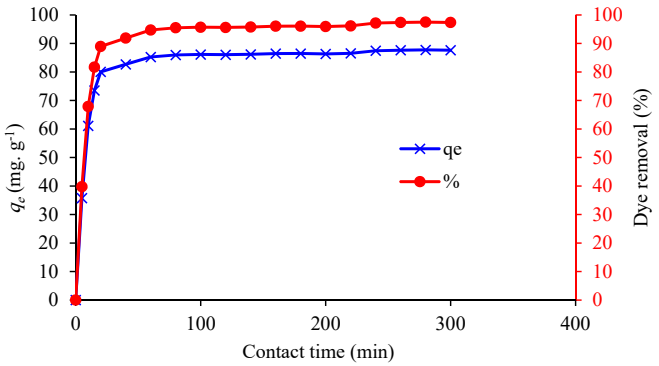

Fig. 11: Effect of contact time on MB adsorption by Fe_3O_4/C (C_0 = 30 mg. L^{-1}, solution volume = 30 mL)

L^{-1} MB and the solution was shacked with 200 rpm for various contact time (up to 300 min). Fig. 11 shows the result of this experiment. It is observed that with increasing contact time, adsorption of MB increases, but after time about 60 min q_e and dye removal remain almost constant. So, this time was used as adsorption time for the rest of the experiments.

Effect of Temperature

Fig. 12 shows the effect of temperature on dye adsorption by two nano-adsorbents (Fe_3O_4 and Fe_3O_4/C). Experiments were carried out at different temperatures (25, 35, 45, 55, and 65 °C), all other parameters in the experiment were kept constant (dosage: 10 mg, dye concentration: 70 mg L^{-1} and pH=10). Results show that by increasing temperature the adsorption capacity of MB increases may be due to an acceleration in the mobility of the MB molecules and consequently enhancement of its interaction with the active sites of the nano-adsorbent surface.

Effect of Initial Dye Concentration

The effect of initial MB concentration on its removal by Fe_3O_4 and Fe_3O_4/C nano-adsorbent was investigated in the concentrations between 20 to 100 mg. L^{-1} (Fig. 13). The result shows that when the initial concentration of MB increases, dye removal percent decreases, which perhaps be due to the saturation of the adsorption sites on the adsorbent surface. On the other hand, with increasing dye concentration, adsorption capacity increases, because at higher concentrations the adsorption equilibrium (MB + Sorbent « MB-Sorbent) moves to the right. Fig. 14 shows a photograph of the

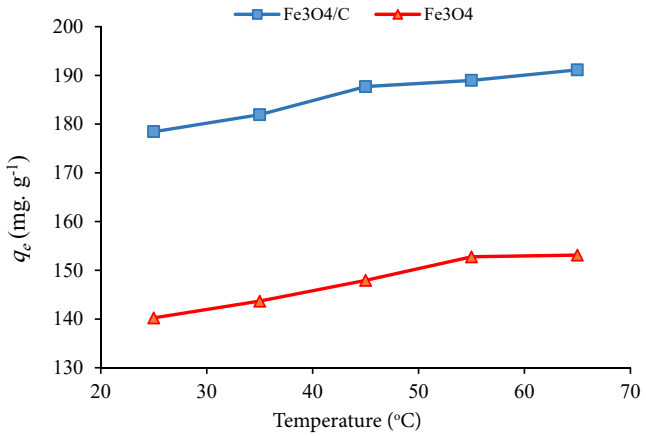

Fig. 12: Effect of temperature on dye adsorption (experimental conditions: dosage = 10 mg at pH =10, volume of solution = 30 mL, dye concentration = 70 mg. L^{-1})

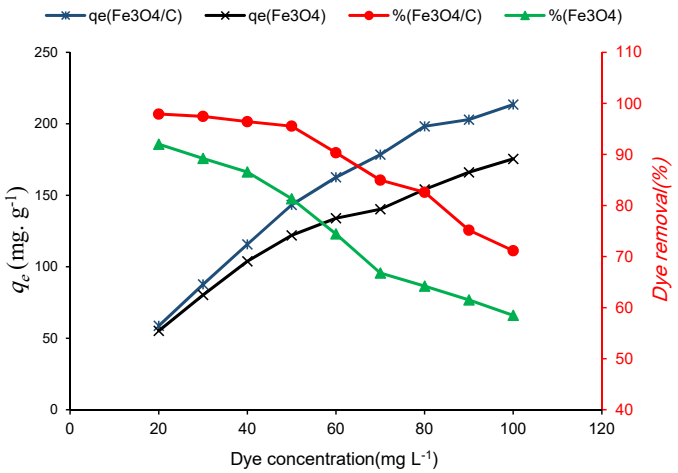

Fig. 13: Effect of dye concentration on the removal of MB

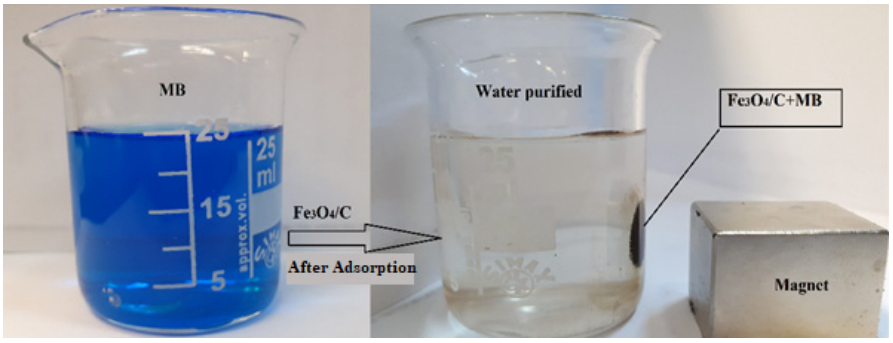

Fig. 14: Photograph of MB adsorption with Fe_3O_4/C Nanocomposite and separation of nano-adsorbent by an external magnet

dye adsorption by Fe_3O_4/C nano sorbent. In this experiment, the nanospheres were dispersed in the dye solution, and after some minutes MB was adsorbed and magnetic NPs were separated easily by an external magnet.

Adsorption Isotherm Study

Equilibrium adsorption in this research was done by 30 mL solutions containing dye with different initial concentrations (20 to 100 mg. L^{-1}) with 10 mg of nano-adsorbent for a period of 180 min.

Adsorption isotherm is one of the significant parameters in the adsorption process. In the present study, three available and major models (Langmuir, Freundlich, and Temkin) were studied to describe the adsorption equilibrium. Langmuir adsorption isotherm has the most application in adsorbing pollutants from the aqueous solutions. If experimental results fitted with Langmuir isotherm model it reveals that dye adsorption on the adsorbent has been done as a monolayer with uniform distribution on active sites of the outer surface of the adsorbent [41, 42] and there isn't any interaction between the dye molecules. In this model, a linear relation is between $1/q_e$ and $1/C_e$ as the following equation:

$$\frac{1}{q_e} = \frac{1}{q_m} + \frac{1}{bq_m C_e} \quad (4)$$

Which C_e is the concentration of dye in equilibrium conditions (mg. L^{-1}), q_e is the adsorbed value of dye at equilibrium concentration (mg. g^{-1}), q_m is the maximum capacity as monolayer adsorption on adsorbent (mg. g^{-1}), and b is the Langmuir constant that depends on the adsorption energy (L. mg^{-1}).

R_L is an important factor, specifies adsorption shape that defined in equation (5) with details (Table 1). In this formula, K_L (L. mg^{-1}) and C_0 (mg. L^{-1}) are Langmuir isotherm constant and initial dye concentration, respectively.

Calculation of R_L values on to Fe_3O_4/C Nanocomposite and Fe_3O_4 NPs show that $0 < R_L > 1$, so adsorption occurs normally and it is a favorable adsorption for two nano-adsorbent (Table 1) [43].

$$R_L = \frac{1}{[1 + K_l C_0]} \quad (5)$$

Freundlich model is used to describe a heterogeneous adsorption process, and the amount of materials that are adsorbed is not limited to a monolayer adsorption, which describes the reversible adsorption process [44]. In the Freundlich model a linear relation is between ln q_e and ln C_e (equation 6):

$$lnq_e = lnK_f + \frac{1}{n} lnC_e \quad (6)$$

In this equation, K_f and n are the Freundlich constants which are related to the system's characteristics.

In Temkin model, it is assumed that the heat of

Table 1: R_L values for determination of the nature of dye adsorption

R_L value	Nature of dye adsorption
R_L>1	Unfavorable (desorption occurs in during the adsorption process)
R_L=1	Linear (isotherm is totally a straight line)
0<R_L>1	Favourable (process adsorption occurs normally under tested conditions)
R_L=0	Irreversible (adsorption is still too strong)

adsorption increases linearly with coverage due to adsorbent–adsorbate interactions [45]. It is expressed linearly as equation (7):

$$q_e = BlnA + BlnC_e \quad (7)$$

Where A is the equilibrium binding constant (L. mg^{-1}) in accordance with the constant B ($B = RT/b$) and maximum binding energy is the Temkin isotherm energy that is related to the heat of adsorption. R is the gas constant (8.314 J. mol^{-1}. K^{-1}), T is the absolute temperature (K), and b is a constant (adsorption enthalpy). Fig. 15 shows the plots of three isotherms (Langmuir, Freundlich, and Temkin) for the MB adsorption on to nano-adsorbent and the related values of parameters and constants for these isotherms are presented in Table 2. As the results show, the obtained data better fitted to a Langmuir isotherm (for Fe_3O_4, R^2 = 0.9902 and Fe_3O_4/C, R^2 = 0.9962) compared to the other isotherms (Freundlich and Temkin).

Thermodynamic and Mechanistic Studies

For the study of the nature and spontaneity of dye adsorption process, the thermodynamic parameters were investigated. they include energy change ($\Delta G°$), enthalpy change ($\Delta H°$), and entropy change ($\Delta S°$) were mentioned in the following equations (8, 9, 10). The values of $\Delta H°$ and $\Delta S°$ were calculated from the slope and intercept of the plot ln K_d vs. $1/T$.

$$K_d = \frac{q_e}{C_e} \quad (8)$$

$$\ln K_d = \frac{\Delta S°}{R} - \frac{\Delta H°}{RT} \quad (9)$$

$$\Delta G° = -RT \ln K_d \quad (10)$$

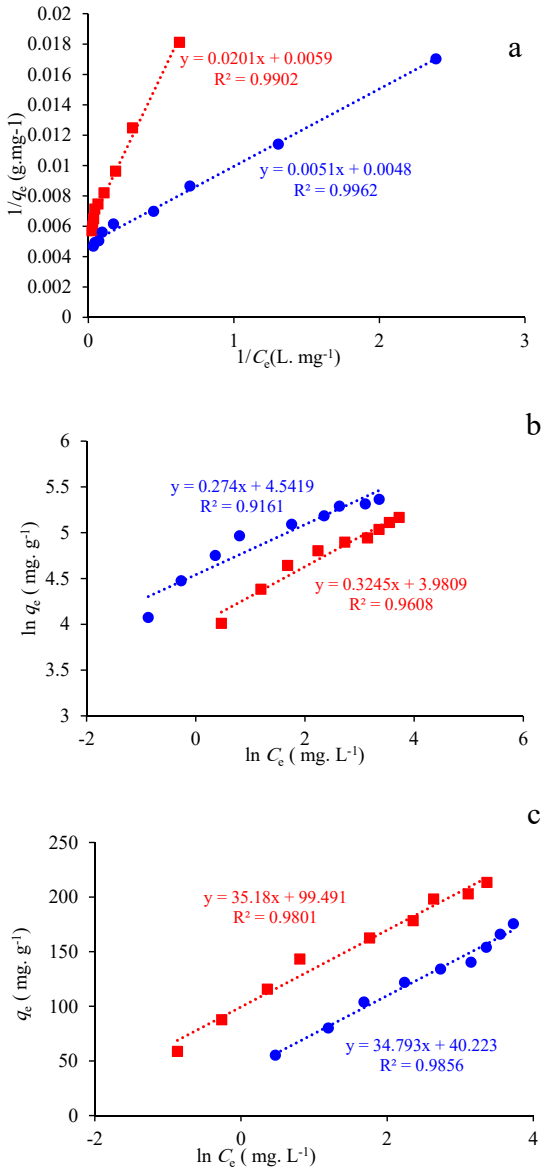

Fig.15: Langmuir (a), Freundlich (b) and Temkin (c) adsorption isotherms for MB adsorption on Fe_3O_4 (■) and Fe_3O_4/C (●) at 298 K

Table 2: Langmuir, Freundlich and Temkin parameters for MB adsorption on Fe_3O_4 (a) and Fe_3O_4/C (b) at 298 K

Model	Parameters	Value	
Langmuir isotherm	q_e (mg. g^{-1})	169.50 [a]	208.33 [b]
	b (L.mg^{-1})	0.29	0.94
	R_L	0.254	0.096
	R^2	0.990	0.996
Freundlich isotherm	K_f [(mg. g^{-1}) (L)] /mg)$^{1/n}$]	93.86	53.56
	n	3.64	3.08
	R^2	0.960	0.916
Temkin isotherm	K_T	3.177	16.91
	b_T	71.24	70.46
	R^2	0.985	0.980

Where K_d is the equilibrium constant, R (8.314 J mol^{-1} K^{-1}) is the universal gas constant, T (K) is the absolute temperature, q_e (mg g^{-1}) is the amount of adsorbate adsorbed at equilibrium and C_e (mg L^{-1}) is the equilibrium concentration. The value of Gibbs free energy (ΔG^o) was calculated by Eq. (10) [46]. The results of these calculations are presented in Table 3.

For two adsorbents negative values of $\Delta G°$ shows the dye adsorption is a spontaneous and feasibility process. Positive values of $\Delta S°$ shows the increase in randomness at the solid–solution interface during the MB adsorption process. The values of enthalpy for dye adsorption ($\Delta H°$) is positive that shows the endothermic nature of the adsorption process. This value for Fe_3O_4 and Fe_3O_4/C is 7.05 and 12.65 respectively, which are less than 40 kJ. mol^{-1} and indicates the adsorption of MB onto magnetic adsorbent is physisorption [47]. With regard to the functional groups in the nano-adsorbent (C-O, OH, C=O), and functional groups in MB (N-R, S-R), an attractive link by hydrogen bonding and Van der Waals interactions is possible, and with the presence of the positive charge on methylene blue there is also the possibility of creating an electrostatic bond.

Kinetic Studies

Adsorption kinetic models are used for determination of the mechanisms controlling the dyes adsorption from an aqueous solution. In this study, two kinetic models were adopted to match the obtained data from experimental. The first adopted method is a Lagergren pseudo-first-order [48]], which is used widely and explained by the following formula:

$$\frac{dq_t}{dt} = k_1(q_e - q_t) \quad (11)$$

In equation (11) q_t is the adsorption capacity (mg. g^{-1}) at time t and k_1 is the rate constant for pseudo-first order model (min^{-1}). Integrating this equation generates the equation (12), that k_1 and q_e are achieved by drawing the ln ($q_e - q_t$) vs. t

$$\ln(q_e - q_t) = lnq_e - \frac{k_1 t}{2.303} \quad (12)$$

The second model is a pseudo-second-order kinetic, presented as:

$$\frac{dq_t}{dt} = k_2(q_e - q_t)^2 \quad (13)$$

Where, k_2 is the rate constant of pseudo-second-order equation (g. mg^{-1}. min^{-1}) and for the other parameters, they have their usual meanings. In this model, it is assumed that the rate of concentration change moment over time is directly proportional to the difference in saturation concentration and moment saturation concentration [49, 50]. Assuming $q_t = 0$ at $t = 0$ integration of the equation (14) gives the following equation:

Table 3: Thermodynamics parameters for adsorption of MB on to magnetic nano-adsorbents

Adsorbent	Dye concentration (mg. L^{-1})	$\Delta H°$ (kJ. mol^{-1})	$\Delta S°$ (J. mol^{-1}. K^{-1})	$\Delta G°$ (kJ. mol^{-1}) at different temperatures (°C)				
				25 °C	35	45	55	65
Fe_3O_4	70	6.66	37.29	-4.45	-4.79	-5.20	-5.67	-5.87
Fe_3O_4/C	70	12.55	65.70	-7.01	-7.60	-8.53	-8.98	-9.59

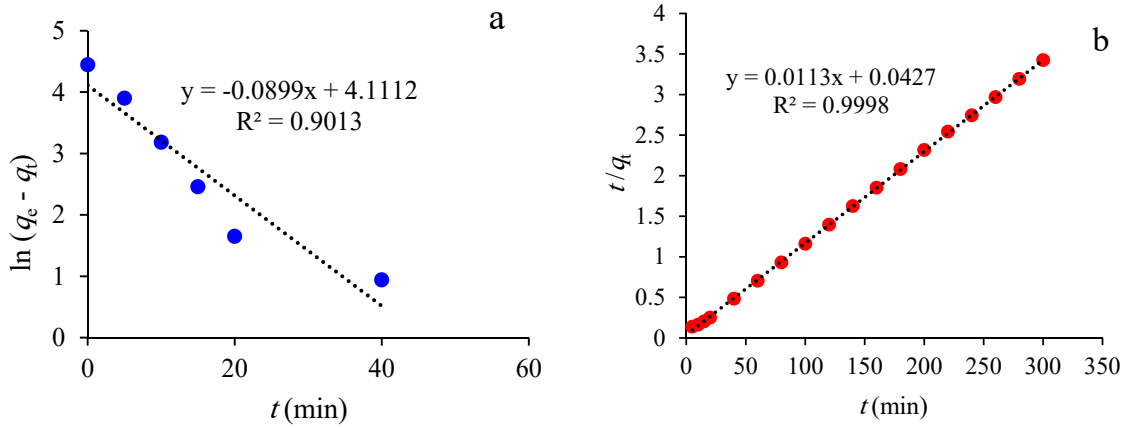

Fig. 16: Pseudo-first-order (a) and pseudo-second-order (b) MB adsorption plots on Fe_3O_4/C

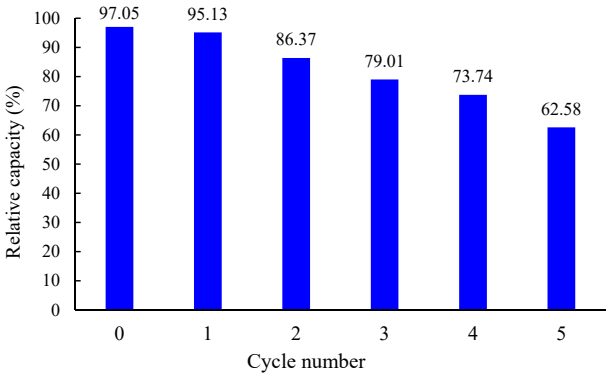

Fig. 17: Regeneration of Fe_3O_4/C Nanocomposite

Table 4: Kinetic data for the MB adsorption on Fe_3O_4/C Nanocomposite

Kinetic model	Parameters
Pseudo-first order	R^2 = 0.9013
	k_1 (min^{-1}) = 0.2070
	q_e (mg. g^{-1}) = 61.01
Pseudo-second order	R^2 = 0.9998
	k_2 (mg. (g. min^{-1}) = 0.0029
	q_e (mg. g^{-1}) = 88.49

Table 5: Comparing of the proposed adsorbent with several recently reported magnetic adsorbents for MB removal

Sorbent	q_{max} (mg . g^{-1})	Reference
B-Fe_3O_4@C	42.11	[29]
Fe_3O_4 NPs (Combustion synthesis)	25.54	[23]
Fe_3O_4/C (Synthesis in two-step)	44.38	[28]
Fe_3O_4 (2D nanolamellar)	77.39	[49]
Fe_3O_4@MIL-100(Fe)	221	[50]
Magnetic graphene-carbon nanotube	65.79	[51]
Fe_3O_4/activated montmorillonite	106.38	[52]
Magnetic loaded carbon	357.1	[53]
Fe_3O_4/activated carbon	321	[54]
Mesoporous Fe_3O_4 NPs	169.50	This work
Mesoporous Fe_3O_4/C Nanocomposite	208.33	This work

$$\frac{t}{q_t} = \frac{1}{k_2 q_e^2} + \frac{t}{q_e} \quad (14)$$

Fig. 16 shows the plots of pseudo-first and pseudo-second-order models, which as obvious the removal of MB by adsorbent follows a pseudo-second-order kinetic (R^2 = 0.9998), and the related kinetic results are reported in Table 4.

Recycling of Adsorbent and Desorption of Dye

One advantage of the proposed nano-adsorbent is easy separation from soluble waste and reuse it by magnet without centrifugation or filtration. For this purpose, amount of 10 mg Fe_3O_4/C in 30 mL solution of dye with 30 mg. L^{-1} concentration was used for dye removal in optimum parameters. After the separation of Fe_3O_4/C nano-adsorbent easily recoverable by washing with diluted HCl water solution. The relative adsorption capacity was calculated referring to the Fe_3O_4/C Nanocomposite without recycling. The result of this study is shown in Fig. 17. As illustrated in this Figure by recycling of Fe_3O_4/C as a magnetic nano sorbent from solution, adsorption capacity decreases. After the first use, the relative adsorbent capacity was 95.13%,

and after 5 cycles this value decreased to 62.58%. Although by recycling the adsorption capacity decreases, but according to low-cost, nontoxic and ease of preparation, Fe_3O_4/C Nanocomposite could be a good adsorbent for dye removal.

Table 5 compares several recently reported magnetic adsorbents for MB removal, with the proposed adsorbent. As this table shows the proposed adsorbent has the better q_{max} than most of these adsorbents.

CONCLUSIONS

In summary, mesoporous Fe_3O_4 and Fe_3O_4/C nanomaterials were synthesized by a hydrothermal method and characterized by various methods such as FT-IR, FE-SEM, TEM, VSM, XRD, EDX, and BET. These nanomaterials were used for removal of the MB cationic dye from water and showed a good adsorption capacity in alkaline pH. Thermodynamic parameters (ΔG^o, ΔH^o, and ΔS^o) were investigated that showed a spontaneous and endothermic adsorption process. The adsorption isotherm had the better fit with Langmuir isotherm, and the kinetic studies indicate that the adsorption of MB on the proposed adsorbent follows a pseudo-second-order kinetic model. Due to its low cost, ease of preparation and high adsorption capacity the proposed magnetic NPs can be considered as an excellent adsorbent for cationic dye removal.

ACKNOWLEDGMENTS

As authors of the article, we gratefully acknowledge the support of this report by the Research Council of Iran University of Science and Technology.

CONFLICTS OF INTEREST

The authors declare that there are no conflicts of interest.

REFERENCES

1. Nekouei F, Nekouei S. Comparative evaluation of BiOCl–NPls–AC composite performance for methylene blue dye removal from solution in the presence/absence of UV irradiation: Kinetic and isotherm studies. Journal of Alloys and Compounds. 2017;701:950-66.
2. Olakunle MO, Inyinbor AA, Dada AO, Bello OS. Combating dye pollution using cocoa pod husks: a sustainable approach. International Journal of Sustainable Engineering. 2017;11(1):4-15.
3. Bilal M, Asgher M, Parra-Saldivar R, Hu H, Wang W, Zhang X, et al. Immobilized ligninolytic enzymes: An innovative and environmental responsive technology to tackle dye-based industrial pollutants – A review. Science of The Total Environment. 2017;576:646-59.
4. Shojaei, S., et al., Removal of Reactive Red 198 by Nanoparticle Zero Valent Iron in the Presence of Hydrogen Peroxide. Journal of Water and Environmental Nanotechnology, 2017. 2(2): p. 129-135.
5. Yang R, Li D, Li A, Yang H. Adsorption properties and mechanisms of palygorskite for removal of various ionic dyes from water. Applied Clay Science. 2018;151:20-8.
6. Khan EA, Shahjahan, Khan TA. Adsorption of methyl red on activated carbon derived from custard apple (Annona squamosa) fruit shell: Equilibrium isotherm and kinetic studies. Journal of Molecular Liquids. 2018;249:1195-211.
7. Rajabi M, Moradi O, Zare K. Kinetics adsorption study of the ethidium bromide by graphene oxide as adsorbent from aqueous matrices. International Nano Letters. 2017;7(1):35-41.
8. Papegowda PK, Syed AA. Isotherm, Kinetic and Thermodynamic Studies on the Removal of Methylene Blue Dye from Aqueous Solution Using Saw Palmetto Spent. International Journal of Environmental Research. 2017;11(1):91-8.
9. Lyu H, Gao B, He F, Zimmerman AR, Ding C, Tang J, et al. Experimental and modeling investigations of ball-milled biochar for the removal of aqueous methylene blue. Chemical Engineering Journal. 2018;335:110-9.
10. Alizadeh N, Shariati S, Besharati N. Adsorption of Crystal Violet and Methylene Blue on Azolla and Fig Leaves Modified with Magnetite Iron Oxide Nanoparticles. International Journal of Environmental Research. 2017;11(2):197-206.
11. Lou T, Cui G, Xun J, Wang X, Feng N, Zhang J. Synthesis of a terpolymer based on chitosan and lignin as an effective flocculant for dye removal. Colloids and Surfaces A: Physicochemical and Engineering Aspects. 2018;537:149-54.
12. Xu J, Xu D, Zhu B, Cheng B, Jiang C. Adsorptive removal of an anionic dye Congo red by flower-like hierarchical magnesium oxide (MgO)-graphene oxide composite microspheres. Applied Surface Science. 2018;435:1136-42.
13. Mohammadi, A. and A. Aliakbarzadeh Karimi, Methylene Blue Removal Using Surface-Modified TiO2 Nanoparticles: A Comparative Study on Adsorption and Photocatalytic Degradation. Journal of Water and Environmental Nanotechnology, 2017. 2(2): p. 118-128.
14. Najafi F, Norouzi M, Zare K, Fakhri A. Removal of ethidium bromide by carbon nanotube in aqueous solution: isotherms, equilibrium mechanism studies, and its comparison with nanoscale of zero valent iron as adsorbent. Journal of Nanostructure in Chemistry. 2013;3(1):60.
15. Liu Y, Chen L, Yang Y, Li M, Li Y, Dong Y. The efficient removal of Cu(II) from aqueous solutions by Fe 3 O 4 @ hexadecyl trimethoxysilane@chitosan composites. Journal of Molecular Liquids. 2016;219:341-9.
16. Zolgharnein J, Choghaei Z, Bagtash M, Feshki S, Rastgordani M, Zolgharnein P. Nano-Fe3O4and corn cover composite for removal of Alizarin Red S from aqueous solution: characterization and optimization investigations. Desalination and Water Treatment. 2016:1-14.
17. Indira T, Lakshmi P. Magnetic nanoparticles–a review. International Journal of Pharmaceutical Sciences and Nanotechnology 2010; 3(3): 1035-42.
18. Hariani PL, Faizal M, Ridwan R, Marsi M, Setiabudidaya D. Synthesis and Properties of Fe3O4 Nanoparticles

by Co-precipitation Method to Removal Procion Dye. International Journal of Environmental Science and Development. 2013:336-40.
19. Todaka Y, Nakamura M, Hattori S, Tsuchiya K, Umemoto M. Synthesis of Ferrite Nanoparticles by Mechanochemical Processing Using a Ball Mill. MATERIALS TRANSACTIONS. 2003;44(2):277-84.
20. Ai Z, Deng K, Wan Q, Zhang L, Lee S. Facile Microwave-Assisted Synthesis and Magnetic and Gas Sensing Properties of Fe3O4 Nanoroses. The Journal of Physical Chemistry C. 2010;114(14):6237-42.
21. Ni S, Lin S, Pan Q, Yang F, Huang K, He D. Hydrothermal synthesis and microwave absorption properties of Fe3O4nanocrystals. Journal of Physics D: Applied Physics. 2009;42(5):055004.
22. Chen D, Ni S, Chen Z. Synthesis of Fe3O4 nanoparticles by wet milling iron powder in a planetary ball mill. China Particuology. 2007;5(5):357-8.
23. Păcurariu C, Paşka O, Ianoş R, Muntean SG. Effective removal of methylene blue from aqueous solution using a new magnetic iron oxide nanosorbent prepared by combustion synthesis. Clean Technologies and Environmental Policy. 2015;18(3):705-15.
24. Datta D, Sah S, Rawat N, Kumar R. Application of Magnetically Activated Carbon for the Separation of Nicotinic Acid from Aqueous Solution. Journal of Chemical & Engineering Data. 2017;62(2):712-9.
25. Cazetta AL, Pezoti O, Bedin KC, Silva TL, Paesano Junior A, Asefa T, et al. Magnetic Activated Carbon Derived from Biomass Waste by Concurrent Synthesis: Efficient Adsorbent for Toxic Dyes. ACS Sustainable Chemistry & Engineering. 2016;4(3):1058-68.
26. Kakavandi B, Jonidi A, Rezaei R, Nasseri S, Ameri A, Esrafily A. Synthesis and properties of Fe3O4-activated carbon magnetic nanoparticles for removal of aniline from aqueous solution: equilibrium, kinetic and thermodynamic studies. Iranian Journal of Environmental Health Science & Engineering. 2013;10(1):19.
27. Do MH, Phan NH, Nguyen TD, Pham TTS, Nguyen VK, Vu TTT, et al. Activated carbon/Fe3O4 nanoparticle composite: Fabrication, methyl orange removal and regeneration by hydrogen peroxide. Chemosphere. 2011;85(8):1269-76.
28. Zhang Z, Kong J. Novel magnetic Fe3O4@C nanoparticles as adsorbents for removal of organic dyes from aqueous solution. Journal of Hazardous Materials. 2011;193:325-9.
29. Qu L, Han T, Luo Z, Liu C, Mei Y, Zhu T. One-step fabricated Fe3O4@C core–shell composites for dye removal: Kinetics, equilibrium and thermodynamics. Journal of Physics and Chemistry of Solids. 2015;78:20-7.
30. Wang F. Novel high performance magnetic activated carbon for phenol removal: equilibrium, kinetics and thermodynamics. Journal of Porous Materials. 2017;24(5):1309-17.
31. Datta D, Kerkez Kuyumcu Ö, Bayazit ŞS, Abdel Salam M. Adsorptive removal of malachite green and Rhodamine B dyes on Fe3O4/activated carbon composite. Journal of Dispersion Science and Technology. 2016;38(11):1556-62.
32. Ranjithkumar V, Hazeen AN, Thamilselvan M, Vairam S. Magnetic Activated Carbon-Fe_3O_4 Nanocomposites—Synthesis and Applications in the Removal of Acid Yellow Dye 17 from Water. Journal of Nanoscience and Nanotechnology. 2014;14(7):4949-59.
33. Sahu UK, Sahu S, Mahapatra SS, Patel RK. Cigarette soot activated carbon modified with Fe 3 O 4 nanoparticles as an effective adsorbent for As(III) and As(V): Material preparation, characterization and adsorption mechanism study. Journal of Molecular Liquids. 2017;243:395-405.
34. Jaafarzadeh N, Kakavandi B, Takdastan A, Kalantary RR, Azizi M, Jorfi S. Powder activated carbon/Fe3O4 hybrid composite as a highly efficient heterogeneous catalyst for Fenton oxidation of tetracycline: degradation mechanism and kinetic. RSC Advances. 2015;5(103):84718-28.
35. He P, Yang K, Wang W, Dong F, Du L, Liu H. Nanosized Fe3O4-modified activated carbon for supercapacitor electrodes. Russian Journal of Electrochemistry. 2013;49(4):354-8.
36. Wang Y, He P, Zhao X, Lei W, Dong F. Coal tar residues-based nanostructured activated carbon/Fe3O4 composite electrode materials for supercapacitors. Journal of Solid State Electrochemistry. 2013;18(3):665-72.
37. Du X, Wang C, Chen M, Jiao Y, Wang J. Electrochemical Performances of Nanoparticle Fe3O4/Activated Carbon Supercapacitor Using KOH Electrolyte Solution. The Journal of Physical Chemistry C. 2009;113(6):2643-6.
38. Khoshsang H, Ghaffarinejad A, Kazemi H, Wang Y, Arandiyan H. One-pot synthesis of S-doped Fe2O3/C magnetic nanocomposite as an adsorbent for anionic dye removal: equilibrium and kinetic studies. Journal of Nanostructure in Chemistry. 2017;8(1):23-32.
39. Verma V, Verma P, Ray P, Ray AR. 2, 3-Dihydrazone cellulose: Prospective material for tissue engineering scaffolds. Materials Science and Engineering: C. 2008;28(8):1441-7.
40. Feng L, Cao M, Ma X, Zhu Y, Hu C. Superparamagnetic high-surface-area Fe3O4 nanoparticles as adsorbents for arsenic removal. Journal of Hazardous Materials. 2012;217-218:439-46.
41. Zauro SA, Vishalakshi B. Amphoteric gellan gum-based terpolymer–montmorillonite composite: synthesis, swelling, and dye adsorption studies. International Journal of Industrial Chemistry. 2017;8(3):345-62.
42. chaudhary S, Sharma J, Kaith BS, yadav S, Sharma AK, Goel A. Gum xanthan-psyllium-cl-poly(acrylic acid-co-itaconic acid) based adsorbent for effective removal of cationic and anionic dyes: Adsorption isotherms, kinetics and thermodynamic studies. Ecotoxicology and Environmental Safety. 2018;149:150-8.
43. Torabinejad A, Nasirizadeh N, Yazdanshenas ME, Tayebi H-A. Synthesis of conductive polymer-coated mesoporous MCM-41 for textile dye removal from aqueous media. Journal of Nanostructure in Chemistry. 2017;7(3):217-29.
44. Mary Ealias A, Saravanakumar MP. Facile synthesis and characterisation of AlNs using Protein Rich Solution extracted from sewage sludge and its application for ultrasonic assisted dye adsorption: Isotherms, kinetics, mechanism and RSM design. Journal of Environmental Management. 2018;206:215-27.
45. Tuzen M, Sarı A, Saleh TA. Response surface optimization, kinetic and thermodynamic studies for effective removal of rhodamine B by magnetic AC/CeO 2 nanocomposite. Journal of Environmental Management. 2018;206:170-7.
46. Aichour A, Zaghouane-Boudiaf H, Iborra CV, Polo MS. Bioadsorbent beads prepared from activated biomass/alginate for enhanced removal of cationic dye from water medium: Kinetics, equilibrium and thermodynamic studies. Journal of Molecular Liquids. 2018;256:533-40.

47. Sun P, Xu L, Li J, Zhai P, Zhang H, Zhang Z, et al. Hydrothermal synthesis of mesoporous Mg 3 Si 2 O 5 (OH) 4 microspheres as high-performance adsorbents for dye removal. Chemical Engineering Journal. 2018;334:377-88.
48. Ahmad R, Mirza A. Synthesis of Guar gum/bentonite a novel bionanocomposite: Isotherms, kinetics and thermodynamic studies for the removal of Pb (II) and crystal violet dye. Journal of Molecular Liquids. 2018;249:805-14.
49. Wang J, Xu J, Wu N. Kinetics and equilibrium studies of methylene blue adsorption on 2D nanolamellar Fe3O4. Journal of Experimental Nanoscience. 2017;12(1):297-307.
50. Aslam S, Zeng J, Subhan F, Li M, Lyu F, Li Y, et al. In situ one-step synthesis of Fe 3 O 4 @MIL-100(Fe) core-shells for adsorption of methylene blue from water. Journal of Colloid and Interface Science. 2017;505:186-95.
51. Wang P, Cao M, Wang C, Ao Y, Hou J, Qian J. Kinetics and thermodynamics of adsorption of methylene blue by a magnetic graphene-carbon nanotube composite. Applied Surface Science. 2014;290:116-24.
52. Chang J, Ma J, Ma Q, Zhang D, Qiao N, Hu M, et al. Adsorption of methylene blue onto Fe3O4/activated montmorillonite nanocomposite. Applied Clay Science. 2016;119:132-40.
53. Altıntıg E, Altundag H, Tuzen M, Sarı A. Effective removal of methylene blue from aqueous solutions using magnetic loaded activated carbon as novel adsorbent. Chemical Engineering Research and Design. 2017;122:151-63.
54. Yang N, Zhu S, Zhang D, Xu S. Synthesis and properties of magnetic Fe3O4-activated carbon nanocomposite particles for dye removal. Materials Letters. 2008;62(4-5):645-7.